ORIGINAL PAPER

Effects of Lanthanum on Structural and Magnetic Properties of $Sr_{1-x}La_{\frac{2}{3}x}Fe_{12}O_{19}$ Compounds: Theoretical and Experimental Results

J. Matilla-Arias[1] · E. Govea-Alcaide[1,2] [ID] · P. Mariño-Castellanos[3] · F. Rosales-Saiz[1] · I. F. Machado[4] · K. Montero-Rey[5]

Abstract

Pre-reacted powders of M-type strontium hexaferrites with chemical composition $Sr_{1-x}La_{\frac{2}{3}x}Fe_{12}O_{19}$ (x = 0.1, 0.2, 0.3 0.5, 0.6) were obtained from the conventional solid state reaction method. The final consolidation of these powders were performed by using the spark plasma sintering (SPS) technique. The influence of the La^{3+} content on the crystal structure and the magnetic properties of the samples were investigated firstly under the framework of a phenomenological model that predicted the cation substitution/distribution in the Sr and/or Fe sites. The theoretical results indicated that La^{3+} ion mostly occupies the Sr^{2+} site. It was also found that as La content increased, a certain amount of Fe^{2+} ions appear as a consequence of the Fe^{3+} to Fe^{2+} reduction. However, the Fe^{2+} occupied preferably the 12k and 4f1 iron sites. The magnetic properties of the obtained samples were assessed by measurements performed in a vibrating sample magnetometer. Also, X-ray diffraction (XRD) measurements were presented as a complementary characterization. We have found that the magnetic properties of the samples degraded as the La^{3+} content increased and the increase of the Fe_2O_3 impurity phase.

Keywords Strontium hexaferrite · La-doped · Phenomenological model · Cation distribution

1 Introduction

M-type hexaferrites are used in applications such as loudspeakers, windscreen wiper motors, and other small electric motors, as permanent magnets in refrigerator seal gaskets, small motors for cordless appliances, and in automobile applications, etc [1]. One of the most commonly used materials for hard magnets is the M-type strontium hexaferrite (SrM), whose chemical formula is $SrFe_{12}O_{19}$, having excellent magnetic properties, high chemical stability, and relatively low cost [1].

Several investigations have been carried out to study the influence of various dopants on its physical properties of M-type hexaferrites. In particular, the influence on the structural and magnetic properties of the rare earth as dopant element in SrM has been extensively studied. Buzinaro et al. [2] reported that the strontium hexaferrite doped with samarium (Sm^{3+}) in the Sr^{2+} site causes the decrease in the saturation magnetization from about 68.8 emu/g at $x = 0$ to about 60.1 emu/g at $x = 0.10$ may be related to the changes in the valence state of iron from Fe^{3+} to Fe^{2+} in the 12k and 2a sites. Others works also discussed that the partial substitution of Sr^{2+} cations by rare earth elements has been carried out Pr^{3+} [3], Nd^{3+} [3, 4], Eu^{3+} [5], Gd^{3+} and Dy^{3+} [6], and La^{3+} [5–11]. According to the presented studies, the replacement of divalent Sr by trivalent rare earth elements in SrM hexaferrites is associated with a valence change of the Fe^{3+} by Fe^{2+} ions in the different

✉ E. Govea-Alcaide
egoveaalcaide@gmail.com

1 Departamento de Matemática-Física, Facultad de Ciencias Informáticas, Naturales y Exactas, Universidad de Granma Apdo. 21, P. O. Box 85100, Bayamo, Cuba

2 Departamento de Física, Universidade Federal do Amazonas, Av. Gen. Rodrigo Octávio Jordão Ramos, 6.200 - Coroado - Setor Norte do Campus Universitário, Manaus-AM, Brazil

3 Departmento de Química y Física, Universidad de Holguín, Holguín, Cuba

4 Departamento de Engenharia Mecatrônica e Sistemas Mecânicos, Escola Politécnica, Universidade de São Paulo, São Paulo, SP, 05508-900 Brazil

5 Departamento de Física de Materiais e Mecânica, Instituto de Física, Universidade de São Paulo, São Paulo, Brazil

iron sites. Therefore, the physical properties' behavior can be influenced. The valence changes in the preferential sites were supported by the results of the Mössbauer experimental technique. However, to our knowledge, only few theoretical studies about M-type strontium hexaferrites have been reported regarding in relation with the cation distribution in the different crystallographic sites of this crystal structure [12–14].

Therefore, the aim of this work is to investigate the influence of the partial substitution of the Sr^{2+} by La^{3+} ions on the structural and magnetic properties of the $Sr_{1-x}La_{\frac{2}{3}x}Fe_{12}O_{19}$ compounds. The framework of the phenomenological model was reported in our previous work [15], which allow the theoretical prediction of the cation substitution distribution in M-type hexaferrites.

2 Experimental Procedure

Polycrystalline samples of $Sr_{1-x}La_{\frac{2}{3}x}Fe_{12}O_{19}$ (x = 0.1, 0.2, 0.3, 0.5, and 0.6) were prepared by the conventional solid–state reaction method. Powders of $SrCO_3$, La_2O_3, and Fe_2O_3 were mixed at the desired stoichiometric ratios. The mixed powders of each composition were milled for 8 h and calcined in air at 1000 °C for 8 h. The calcined powders were then ground for 4 h and pressed into pellets at 2.6 ton/cm². The obtained pellets were sintered at 1200 °C in air for 45 min. After that, the pellet samples were again reground and these powders will be hereafter referred to as pre-reacted powders.

The final consolidation of the samples was performed in a SPS 1050 Dr Sinter® apparatus manufactured by Sumitomo Coal Mining Co. Ltd., Japan. Pre-reacted powders of $Sr_{1-x}La_{\frac{2}{3}x}Fe_{12}O_{19}$ ($\sim$ 3 g) were placed inside a cylindrical graphite die with dimensions of 50 mm (outer diameter) and 20 mm (inner diameter). Two graphite plungers of $\sim$ 40 mm in height and 20 mm in diameter were placed between the sample, in which the pressure was applied. In order to protect the die and facilitate the sample release after consolidation, graphite foils were inserted between the internal surfaces of the die and between the top and the bottom surfaces of the sample and the graphite plungers. The graphite die was then placed inside the chamber of the SPS apparatus and sintering was conducted under vacuum (from 10 to $\sim$30 Pa). The consolidation temperature, T_D, the holding time, t_D, and the heating rate, T_D/t_r, for all samples were 900 °C, 5 min, and $\sim$ 175 °C/min, respectively. The temperature was measured during the consolidation process by using a (K-type) thermocouple, which was inserted into a small hole in one side of the graphite die. The maximum uniaxial compacting pressure used to synthesize all samples experiments was 50 MPa

reached by a gradual increase during the first 3 min. After the sintering process, each sample was first naturally cool for about 50 min and then removed from the die. The density of all consolidated pellets was determined by using the Archimedes method.

The phase identification of the samples was evaluated from X-ray diffraction patterns obtained in a Bruker-AXS D8 Advance diffractometer. These measurements were performed at room temperature using $CuK\alpha$ radiation in the $3° \leq 2\theta \leq 80°$ range with a 0.05° (2θ) step size, and 5-s counting time.

The magnetization measurements as a function of applied magnetic field $M(H)$ were carried out in a vibrating sample magnetometer (Lakeshore 7404, USA). $M(H)$ data were taken at 300 K and under an applied magnetic field range $-14 \leq H \leq 14$ kOe.

3 Phenomenological Model

The SrM crystal structure has a great number of similar crystallographic sites that can be occupied by the cationic dopants. In this structure, the O^{2-} ions form a hexagonal closed packed lattice and every five oxigen layers, one O^{2-} ion is replaced with Ba^{2+}, Sr^{2+} or Pb^{2+} in BaM, SrM or PbM respectively [16]. Fe^{3+} occupies the interstitial positions of the oxygen lattice [16]. In the unit cell of the SrM, Fe^{3+} ions occupy three octahedral sites (2a, 4f2, and 12k), one tetrahedral (4f1) site, and one bipyramidal (2b) site [16], according to Wyckoff's notation. Also, there are six different sites: one polyhedral site for Sr^{2+} ions (2d) and other five for oxygen ions [17].

The process can be modeled as an interaction process between the cation and the site to be occupied. The model is only valid for low dopant concentrations per unit formula because possible effects due to the distortion of the lattice were not considered [15, 18]. Considering that the doping process obeys statistical laws, the central parameter of the model is the substitution index per site, SI [18]. This parameter can be interpreted as a measure of the site occupation probability of the dopant cation on the ith site and can be defined as [15]:

$$SI_i^{dop} = \prod_{j=1}^{8} F_{i,j}^{dop} \tag{1}$$

where i is the ith-site number

$$F_{i,j}^{dop} = \begin{cases} \frac{1}{\sqrt{2\pi}\sigma_j} \exp\left[-\frac{\Delta m_j^2}{2\sigma_j^2}\right] & \text{if } j = 1-6 \quad (2a) \\ N_i \eta^{dop} \left(1 - \eta^{dop}\right)^{(N_i-1)} & \text{if } j = 7 \quad (2b) \\ nc_i \varrho^{dop} \left(1 - \varrho^{dop}\right)^{(nc_i-1)} & \text{if } j = 8 \quad (2c) \end{cases}$$

In (2a), $\sigma_j = k_e m_j^{hcat}$ is the standard deviation, and $k_e \sim 0.15$ is a value obtained according to Pauling's rules and the specific experimental conditions [19]. Also, $\Delta m_j = m_j^{dop} - m_j^{hcat}$ and m_j can be any of the following factors (see Table 1):

1) the cationic radius, $R_{cat_i} = \alpha_{e_i} R_{ion}$, where α_{e_i} is a coefficient that depends on the coordination number at the ith site, nc_i, and R_{ion} is the ionic radius;
2) the electron's valence, q;
3) the ionic potential, $P_{ion_i} = q/R_{cat_i}$;
4) the electric charge per site, $Q_i = q/nc_i$, where nc_i is the coordination number at the ith site (see Table 1) and
5) the effective atomic number $Z_{eff} = (Z_{cat} - q) + 2nc_i$, where Z_{cat} is the atomic number of the cation;
6 the electronegativity, χ.

Notice that (2a) quantifies the differences between the dopant cation (dop) and the host cation (hcat) that may be Sr^{2+} or Fe^{3+}. Additionally, in (2b) and (2c), a binomial statistical distribution function was introduced to consider the relation between the occupation number of the ion in each site, N_i, and the fraction of dopant concentration, η^{dop}, and the relation between the coordination number of the ion in each site, nc_i, and the fraction of dopant electronic density, ϱ^{dop}.

In the same manner as in (1) and (2a–c), it is possible to define a substitution index per site for the host cation (hcat), SI_i^{hcat}. In this case, the "dopant" cation and the host one are the same ion, i.e., $\Delta m_j = 0$ [18].

$$
F_{i,j}^{hcat} = \begin{cases} \frac{1}{\sqrt{2\pi}\sigma_j} & \text{if } j = 1-6 \ (3a) \\ 1 - N_i\left(1 - \eta^{cat}\right)\left(\eta^{cat}\right)^{(N_i-1)} & \text{if } j = 7 \quad (3b) \\ 1 - nc_i\left(1 - \varrho^{cat}\right)\left(\varrho^{cat}\right)^{(nc_i-1)} & \text{if } j = 8 \quad (3c) \end{cases}
$$

Table 1 Values of the parameters in calculations: the atomic number, Z_{cat}, atomic mass, m_A, the electron's valence, q, the ionic ratio, R_{ion}, and the electronegativity, χ

Ion	Z_{cat}	m_A (g/mol)	q	R_{ion} (Å)	χ (Puling's scale)
Fe^{3+}	26	55.85	3	0.67	1.8
Fe^{2+}	26	55.85	2	0.80	1.8
Sr^{2+}	38	87.63	2	1.32	1.0
O^{2-}	8	16.00	2-	1.40	3.5
La^{3+}	57	138.92	3	1.22	1.1

Site	2a	2b	4f1	4f2	12k	2d
nc_i	6	5	4	6	6	12
N_i	1	1	2	2	6	1

Taking into account all the above considerations makes it possible to define the occupation probability of the dopant and the host cation, respectively, as:

$$
S_i = \begin{cases} \left(\frac{SI_i^{dop}}{SI_i^{dop}+SI_i^{hcat}}\right)\frac{N_i}{\sum N_i} & \text{for dopant cation} \quad (4a) \\ \left(\frac{SI_i^{hcat}}{SI_i^{dop}+SI_i^{hcat}}\right)\frac{N_i}{\sum N_i} & \text{for host cation} \quad (4b) \end{cases}
$$

Also, the site occupation number of the dopant cation can be calculated as:

$$
Q_i^{dop} = N_i - Q_i^{hcat}. \tag{5}
$$

where Q_i^{hcat} is the occupation number of the host cation, which is defined as:

$$
Q_i^{hcat} = \begin{cases} \left(\sum N_i - x\right)\frac{S_i^{hcat}}{\sum S_i^{hcat}} & \text{for Fe sites} \quad (6a) \\ (N_i - x)S_i^{hcat} & \text{for Sr site} \quad (6b) \end{cases}
$$

In all above-mentioned equations, the host cation is referring to Sr^{2+} or Fe^{3+} according to the crystallographic site that occupies the dopant cation.

4 Results and Discussion

Let us first inspect the influence of La^{3+} content on the structural and the phase formation of the M-type strontium ferrite within the framework of the phenomenological model presented above. Figure 1a and b show the occupation probability of La^{3+} in the Sr and Fe sites, respectively. The obtained results indicate that $S_i^{La^{3+}}$ is eleven orders of magnitude higher in Sr site than in Fe; therefore, the La^{3+} should occupy the Sr^{2+} site in the crystal structure. This is not an unexpected result by considering the similitude between Sr^{2+} (host cation) and La^{3+} (dopant cation). However, values of the $S_i^{La^{3+}}$ in Sr site are also low mostly due to the difference between the valences of the La^{3+} and Sr^{2+}. Such a difference also affect the charge neutrality of the samples as a whole, triggering the reduction of Fe^{3+} ions to Fe^{2+}, as reported elsewhere [7, 9]. Under the above result, it is also necessary to investigate the occupation probability of the Fe^{2+} on both the Fe and the Sr sites.

Figure 2a and b show the occupation probability of the Fe^{2+} in the Fe^{3+} and Sr^{2+} sites, respectively. The results indicate that the order of $S_i^{Fe^{2+}}$ is $\sim 10^{-4}$ for the iron

Fig. 1 Probability of occupation of La^{3+} ($S_i^{La^{3+}}$) as function of the concentration (x) per unit formula, for $Sr_{1-x}La_{\frac{2}{3}x}Fe_{12}O_{19}$, with $x = 0, 0.1, 0.2, 0.3, 0.5, 0.6$. **a** Probability of occupation in Sr sites. **b** Probability of occupation in Fe sites
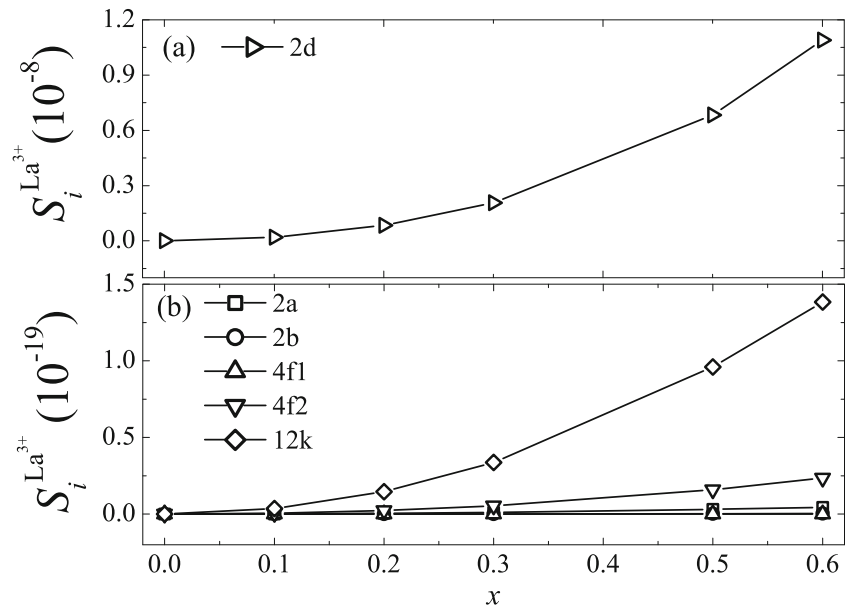

sites, which is higher than the values of the $S_i^{Fe^{2+}}$ in the Sr^{2+} site (see Fig. 2a), even higher than the occupation probability of the La^{3+} in the Sr site (see Fig. 1a). Also, according to the results showed in Fig. 2b, $S_i^{Fe^{2+}}$ increases with increasing of the La^{3+} content being more marked in the 12k site, followed by the 4f1 and 4f2 sites. The above findings suggest that the Fe^{2+} cation occupy the iron sites and not the strontium site inside the crystal structure of the SrM, and that when the SrM is doped with La^{3+} may occur

the valence reduction of Fe^{3+} by Fe^{2+} in the 2a and 4f2 iron sites [7, 9].

We have also studied the influence of the La^{3+} content on the reticular energy, U_{POT}, of the SrM ferrite. In a previous work, the U_{POT} was calculated by using the Eqs. (4)–(7) of Ref. [15]. Additionally, our estimations of the reticular energy were conducted by assuming two physical scenarios: (A) considering only the La^{3+} dopant and (B) taken into account both La^{3+} and Fe^{2+} ions. As observed in the Fig. 3,

Fig. 2 Probability of occupation of Fe^{2+} (S_i^{Fe}) as function of the concentration (x) per unit formula, for $Sr_{1-x}La_{\frac{2}{3}x}Fe_{12}O_{19}$, with $x = 0, 0.1, 0.2, 0.3, 0.5, 0.6$. **a** Probability of occupation in Sr sites. **b** Probability of occupation in Fe sites
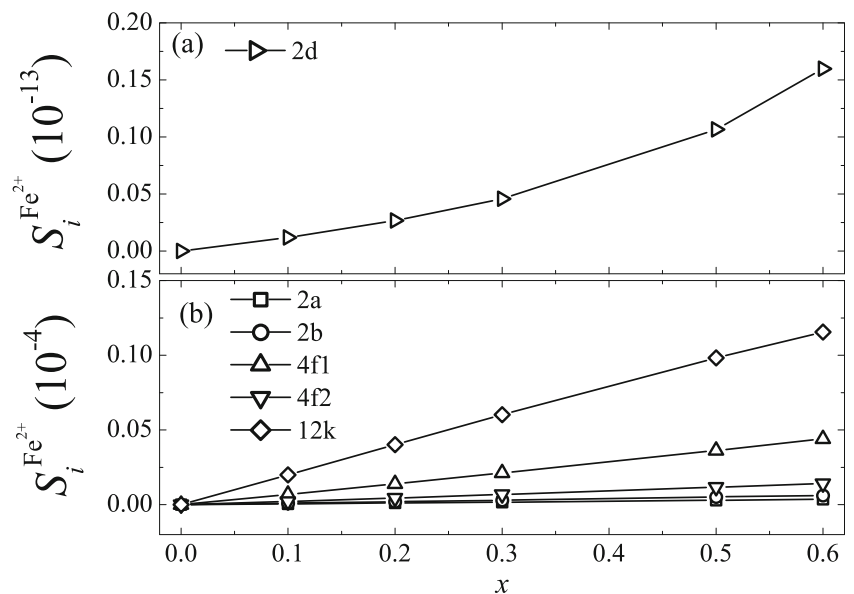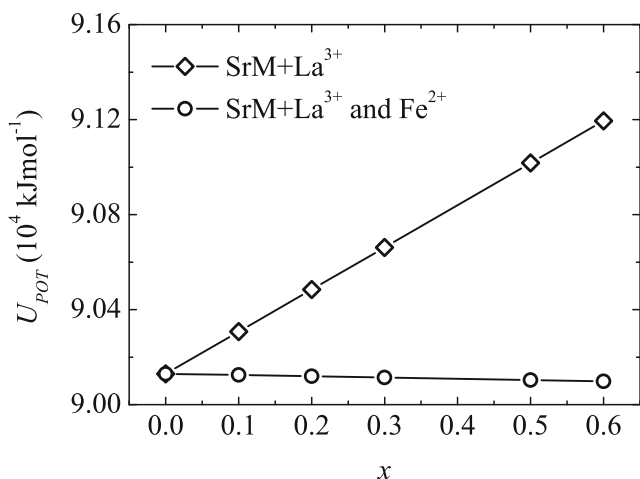
Fig. 3 Reticular energy U_{POT} as function of the La concentration per unit formula, x, for $Sr_{1-x}La_{\frac{2}{3}x}Fe_{12}O_{19}$, with $x = 0, 0.1, 0.2, 0.3, 0.5, 0.6$

if we consider the case A, then the reticular energy of the compound tends to increase with the La content. However, in the case B, the values of U_{POT} are lower than in the case B and slightly decreases with increasing the La content. The above result can be related to the difference of the ionic radius of Fe^{3+} and Fe^{2+}, 0.67Å and 0.80Å, respectively (see Table 1). The Fe^{2+} ions in the SrM ferrite mostly appears in the form of Fe_2O_3 [7, 9], and the reticular energy of Fe_2O_3 is $\sim 1.48 \times 10^4$ kJmol^{-1}, a value six time lower than the reticular energy estimated for the pure $SrFe_{12}O_{19}$ of $\sim 9.02 \times 10^4$ kJmol^{-1}.

We want to remark that the reticular energy for the La-doped SrM ferrite is lower considering the reduction of the Fe^{3+} to Fe^{2+} ions. The above statement can be verified experimentally by the presence of the Fe_2O_3 in XRD analysis as reported elsewhere [7, 9, 20, 21]. Also, taken into account the slight decreases of U_{POT} with increasing the La content (see Fig. 3), the preparation conditions for all samples were the same (see Section 2).

Now, let us check the theoretical findings with the experimental data. Figure 4 shows the X-ray diffraction spectra of $Sr_{1-x}La_{\frac{2}{3}x}Fe_{12}O_{19}$ samples with $x = 0, 0.1,$ 0.2, 0.3, 0.4, 0.5, 0.6. The obtained results shown that most of the indexed reflections belonging to the pure SrM hexaferrite. However, as La^{3+} content increases ($x \geq 0.1$) some impurities of Fe_2O_3 and/or $Sr_2Fe_2O_5$ were detected. The type and the phase content for each value of x are reported in the Table 2. It was found that the amount of Fe_2O_3 increases from $\sim 7\%$ ($x = 0.1$) to $\sim 22\%$ ($x = 0.6$) with increasing the La content. Notice that the presence of this impurity is not an unexpected result as discussed above. In addition, it was not detected La-based impurity or extra

phases for any value of x, suggesting the partial substitution of Sr in the crystal structure. The unit-cell parameters were also calculated from X-ray diffraction reflections and by using the Cohen method. The obtained values are listed in the Table 3. In this case, all values of a and c are in line with those reported elsewhere for the same compound [7]. Also, it was not observed appreciable variations of the above mentioned parameters with increasing the La content.

Values of the theoretical density ρ_{mod} estimated by using the reticular energy U_{POT} (see Eq. (8) in Ref. [15]), which in turn is calculated from the cation distribution obtained from the phenomenological model as above mentioned, and those obtained from XRD diffraction patterns, ρ_{XRD}, for different La content are listed in the Table 3. It is possible to observe from these values that the changes in the density of the compound do not exceed 2.9%. The experimental volume density of the samples after the SPS consolidation, determined by the Archimedes method was $\rho_{exp} \sim 4.75$ g/cm^3. Thus, the relative density ρ_{exp}/ρ_{XRD} is $\sim 92\%$ in all samples. Note that the difference between the experimental density ρ_{exp} and the theoretical density ρ_{mod} estimated by using the phenomenological model results does not exceeded 5.1%.

On the other hand, the magnetic properties are affected by the presence of the Fe_2O_3 impurities, as well as by the Fe^{3+}-Fe^{2+} valence reduction in the iron sites. The room temperature $M(H)$ curves and the magnetic properties of $Sr_{1-x}La_{\frac{2}{3}x}Fe_{12}O_{19}$ samples, with ($0 \leq x \leq 0.6$), are shown in Fig. 5. It can be seen that, in general, when the concentration of dopant per unit formula increased, the saturation magnetization and the remanent magnetization decreased from 57.5 emu/g at x=0 to about 27.1 emu/g at x=0.6 and from 27.7 emu/g at x=0 to about 13.4 emu/g at x=0.6, respectively. According to the results showed in Fig. 5, the lowest values of the magnetic properties (e.g., M_s and M_r) correspond to the samples with $x = 0.2$ (M_s=27.5 emu/g and M_r=10.9 emu/g) and $x = 0.6$, which may be explained by considering that the amount of Fe_2O_3 secondary phase was significantly greater in these samples than the rest, as indicated the intensity of peaks on X-ray pattern in Fig. 4.

Also, SrM hexaferrite have a ferrimagnetic structure with the magnetic moments of the Fe^{3+} cations aligned parallel to each other and to the crystallographic c-axis in 2a, 2b, and 12k, whereas in 4f2 and 4f1 sites, the magnetic moments of the Fe^{3+} cations point in the opposite direction [7]. Therefore, taking into account the collinear array of the magnetic moments in the unit cell of $Sr_{1-x}La_{\frac{2}{3}x}Fe_{12}O_{19}$, the saturation magnetization can be calculated as: $M_s = \sum_{i=1}^{5} \left(\mu^{Fe^{3+}} Q_i^{Fe^{3+}} + \mu^{Fe^{2+}} Q_i^{Fe^{2+}} \right)$.

Fig. 4 X-ray diffraction patterns taken in powder of $Sr_{1-x}La_{\frac{2}{3}x}$ $Fe_{12}O_{19}$ samples. The reflections belonging the $SrFe_{12}O_{19}$ phase are marked by Miller indexes (COD file number: 96-100-6001). Extra phase $Sr_2Fe_2O_5$ and Fe_2O_3 are identified as (+) and (*), respectively
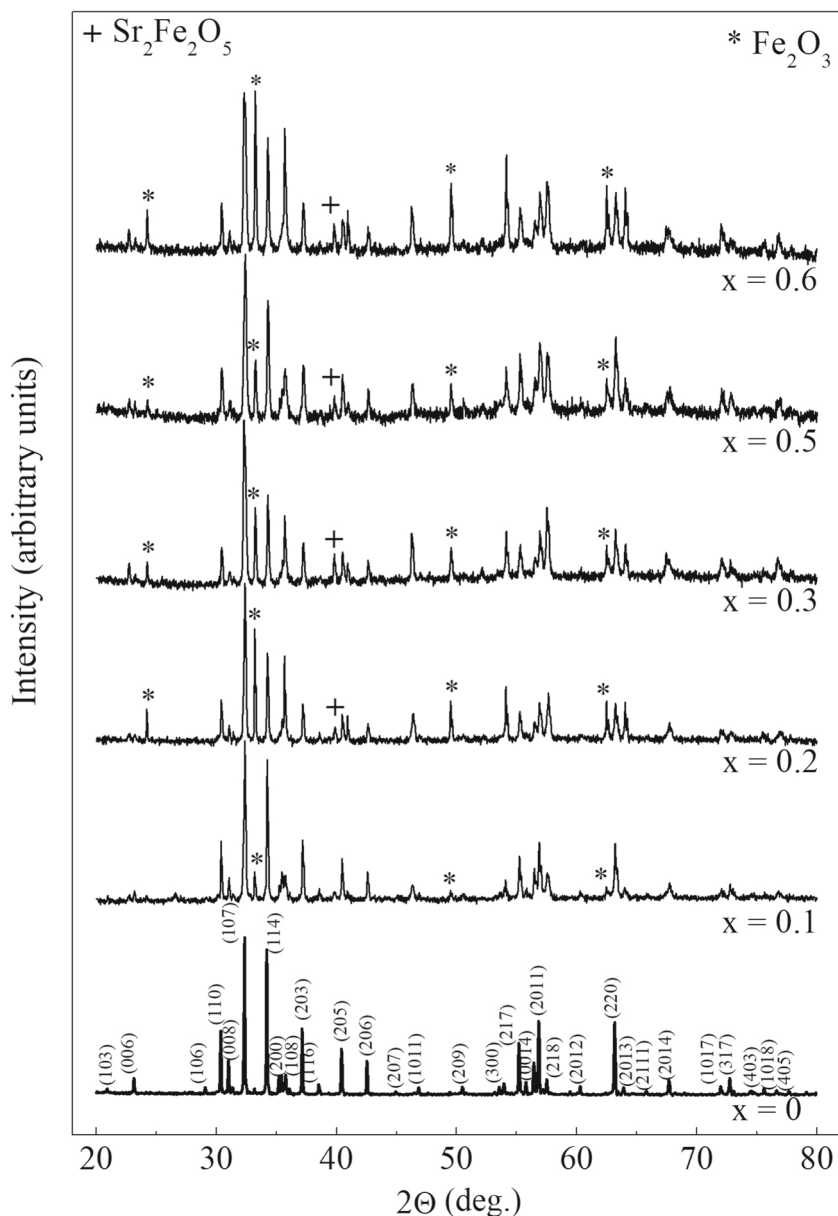
Due to at $T = 0$ K the magnetic moment of the Fe^{3+} ($\mu^{Fe^{3+}} = 5.0\mu_B$) and the magnetic moment of the Fe^{2+} ($\mu^{Fe^{2+}} = 4.0\mu_B$), the decreasing of the saturation magnetization may be attributed mainly to the reduction of Fe^{3+} to Fe^{2+}. As mentioned above (see Fig. 2), such process occurs in 12k spin up sites because the probability of occupation values of the Fe^{2+} cation in this site is higher than the rest of the iron sites. The theoretical magnetization of saturation calculated from the above-mentioned equation, for $x = 0$ and $x = 0.6$, was 20.00 μ_B and 19.87 μ_B, respectively. These results indicated that the diminution of the values of the magnetization of saturation do not exceed 0.65%. However, the experimental values of the

magnetization of saturation for $x = 0$ and $x = 0.6$ were 57.5 emu/g and 27.1 emu/g, respectively, which indicated a diminution of 52.87%, that is much greater than 0.65% obtained from theoretical values above mentioned. It suggests that the decreasing in the magnetization of saturation values was fundamentally result of the presence of the Fe_2O_3 secondary phase in the samples, although for real samples at room temperature, the assumption of the collinear array of magnetic moments in the unit cell is no longer valid.

On the other hand, values of the coercivity H_c were found to increase from 1 to 3 kOe with the increasing of the La content. A result similar to that was reported
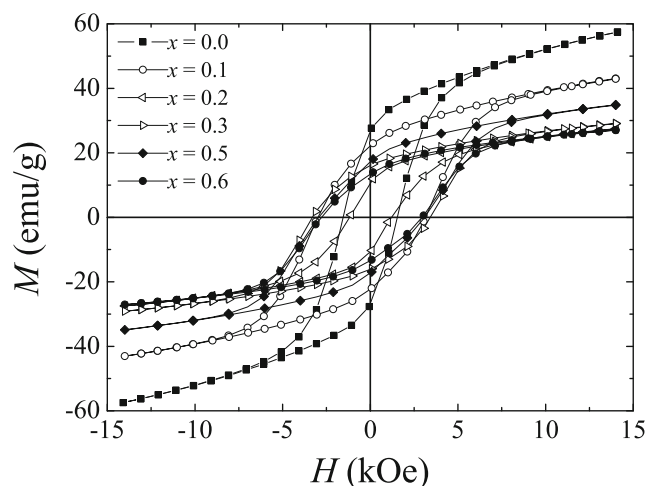
Table 2 Phase composition of $Sr_{1-x}La_{\frac{2}{3}x}Fe_{12}O_{19}$ samples for different values of La content, x

x	Phase composition	Content (%)
0	$SrFe_{12}O_{19}$ (ICCD No. 96-100-6001)	100
0.1	$SrFe_{12}O_{19}$ (ICCD No. 96-100-6001)	92.9
	Fe_2O_3 (ICCD No. 96-210-1168)	7.1
0.2	$SrFe_{12}O_{19}$ (ICCD No. 96-100-6001)	89.1
	Fe_2O_3 (ICCD No. 96-210-1168)	9.7
	$Sr_2Fe_2O_5$ (ICCD No. 96-200-2241)	1.2
0.3	$SrFe_{12}O_{19}$ (ICCD No. 96-100-6001)	85.3
	Fe_2O_3 (ICCD No. 96-210-1168)	13.0
	$Sr_2Fe_2O_5$ (ICCD No. 96-200-2241)	1.7
0.5	$SrFe_{12}O_{19}$ (ICCD No. 96-100-6001)	86.1
	Fe_2O_3 (ICCD No. 96-210-1168)	12.4
	$Sr_2Fe_2O_5$ (ICCD No. 96-200-2241)	1.5
0.6	$SrFe_{12}O_{19}$ (ICCD No. 96-100-6001)	71.8
	Fe_2O_3 (ICCD No. 96-210-1168)	22.1
	$Sr_2Fe_2O_5$ (ICCD No. 96-200-2241)	6.1

Fig. 5 $M-H$ curves of $Sr_{1-x}La_{\frac{2}{3}x}Fe_{12}O_{19}$ samples at room temperature, for each value of concentration (x) per unit formula

elsewhere [6, 7, 10]. Since the coercivity, H_c depends on grain shape, size, distribution, etc [20], the lower value of the coercivity of the sample with $x = 0.2$ may be related to any substantial change on the microstructure for this sample. Additionally, the coercivity enhancement was reported in other ferrites and related to a microstructure with grains with core/shell morphology [22]. We want to point out that the spark-plasma consolidation promotes this kind of morphology because the process occurs under vacuum [23]. In this case, the core should be comprised of stoichiometric $Sr_{1-x}La_{\frac{2}{3}x}Fe_{12}O_{19}$ and the shell could be similar, but oxygen deficiency. However, the existence and a possible relationship between the shell/core morphology and the magnetic properties of these materials must be investigated in details in a future work.

5 Conclusions

High-density samples of $Sr_{1-x}La_{\frac{2}{3}x}Fe_{12}O_{19} \sim 92\%$ were obtained by spark plasma technique. The obtained X-ray diffraction data showed that the presence of the Fe_2O_3 secondary phase increased with La content of the samples. From the results obtained by using of the phenomenological model, it was found that (i) La^{3+} ion only occupies the Sr^{2+} site; (ii) as La content increased, the Fe^{2+} ions appear as a consequence of the Fe^{3+} to Fe^{2+} reduction; and (iii) the Fe^{2+} ion occupies preferably the 12k and 4f1 iron sites. Such a sequence of processes impacts negatively the magnetic properties of SrM compounds.

Table 3 Concentration (x) per unit formula, lattice parameters (a and c), X-ray density (ρ_{XRD}), and theoretical density (ρ_{mod}) of $Sr_{1-x}La_{\frac{2}{3}x}Fe_{12}O_{19}$ samples

x	a (Å)	c (Å)	ρ_{XRD} (g/cm^3)	ρ_{mod} (g/cm^3)
0	5.87	23.05	5.12	4.51
0.1	5.87	23.06	5.16	4.52
0.2	5.87	23.07	5.17	4.54
0.3	5.86	23.05	5.21	4.55
0.5	5.86	23.06	5.27	4.58
0.6	5.87	23.08	5.27	4.59

References

1. Pullar, R.C.: A review of the synthesis, properties and applications of hexaferrite ceramics. Prog. Mater. Sci. **57**, 1191–1334 (2012)
2. Buzinaro, M.A.P., Ferreira, N.S., Cunha, F., Macêdo, M.A.: Hopkinson effect, structural and magnetic properties of M-type Sm^{3+}-doped $SrFe_{12}O_{19}$ nanoparticles produced by a proteic solgel process. Ceram. Int. **42**, 5865–5872 (2016)
3. Lechevallier, L., Le Breton, J.M., Morel, A., Tenaud, P.: On the solubility of rare earths in M-type $SrFe_{12}O_{19}$ hexaferrite compounds. J. Phys.: Condens. Matter. **20**, 175203 (2008)
4. Bhat, B.H., Want, B.: Magnetic behaviour of Neodymium-substituted strontium hexaferrite. Appl. Phys. A **122**, 148 (2016)
5. Berry, F.J., Marco, J.F., Ponton, C.B., Whittle, K.R.: Preparation and characterization of rare earth-doped strontium hexaferrites $Sr_{1-x}M_xFe_{12}O_{19}$ (M=La, Eu). J. Mater. Sci. Lett. **20**, 431–434 (2001)

6. Singh, T., Batra, M.S., Singh, I., Katoch, A.: Composition dependence of the magnetic properties of strontium hexaferrite doped with rare earth ions. J. Phys:. Conf. Series. **534**, 012013 (2014)

7. Liu, X., Zhong, W., Yang, S., Yu, Z., Gu, B., Du, Y.: Influences of La^{3+} substitution on the structure and magnetic properties of M-type strontium ferrites. J. Magn. Magn. Mater. **238**, 207–214 (2002)

8. Küpferling, M., Grössinger, R., Pieper, M.W., Wiesinger, G., Michor, H.: Structural phase transition and magnetic anisotropy of La-substituted M-type Sr hexaferrite. Phys. Rev. B **73**, 144408 (2006)

9. Seifert, D., Töpfer, J., Langenhorst, F., Le Breton, J.-M., Chiron, H., Lechevallier, L.: Synthesis and magnetic properties of La-substituted M-type Sr hexaferrites. J. Magn. Magn. Mater. **321**, 4045–4051 (2009)

10. Azim, M., Atiq, S., Riaz, S., Naseem, S.: Indexing the structural parameters and investigating the magnetic properties of lanthanum doped strontium hexaferrites. IOP Conf. Series:. Mater. Sci. Eng. **60**, 012045 (2014)

11. Wang, Z., Yang, W., Zhou, Z., Jin, M., Xu, J., Sui, Y.: Preparation and magnetic properties of La-substituted strontium hexaferrite by microwave-assisted Sol-Gel method. J. Supercond. Nov. Magn. **29**, 981–984 (2016)

12. Dixit, V., Kim, S.-G., Park, J., Hong, Y.-K.: Effect of ionic substitutions on the magnetic properties of strontium hexaferrite: A fir st principles study. AIP Adv. **7**, 115209 (2017)

13. Dixit, V., Nandadasa, C.N., Kim, S.-G., Kim, S., Park, J., Hong, Y.-K., Liyanage, L.S.I., Moitra, A.: J. Appl. Phys. **117**, 243904 (2015)

14. Dixit, V., Nandadasa, C.N., Kim, S.-G., Kim, S., Park, J., Hong, Y.-K.: J. Appl. Phys. **118**, 203908 (2015)

15. Matilla-Arias, J., Govea-Alcaide, E., Mariño-Castellanos, P., Rosales-Saiz, F.: Phenomenological model for prediction of cation substitution distribution and some physical properties in Mn^{3+}-doped barium hexaferrite. J. Supercond. Nov. Magn. **31**(1), 251–256 (2018)

16. Wohlfarth, E.P.: Handbook of Magnetic Materials, pp. 318–323. North-Holland Publishing Company, Netherlands (1982)

17. Kobayashi, Y., Oda, E., Nishiuchi, T., Nakagawa, T.: Cation distribution analysis of SrLaCo M-type ferrites by neutron diffraction, extended X-ray absorption fine structure and X-ray magnetic circular dichroism. J. Cer. Soc. Jpn. **119**, 285–290 (2011)

18. Mariño-Castellanos, P.A., Moreno, A.C., Orozco, G., Garcia, J.A., Govea-alcaide, E.: Structural and magnetic study of the Ti^{4+}-doped barium hexaferrite ceramic samples: Theoretical and experimental results. Physica. B **406**, 3130–3136 (2011)

19. Chiang, Y.M., Birnie, D.P., Kingery, W.D. (eds.): Physical Ceramics, vol. 522. Wiley, New York (1997)

20. Bolarín-Miró, A.M., Sánchez-De Jesús, F., Cortés-Escobedo, C.A., Díaz-De la Torre, S., Valenzuela, R.: Synthesis of M-type $SrFe_{12}O_{19}$ by mechanosynthesis assisted by spark plasma sintering. J. Alloys. Comp. **643**, S226–S230 (2015)

21. Stingaciu, M., Topole, M., McGuiness, P., Christensen, M.: Magnetic properties of ball-milled $SrFe_{12}O_{19}$ particles consolidated by spark-plasma sintering. Sci. Rep. **5:14112**, 1–8 (2015)

22. Cui, W., Zhang, T., Zhou, X., Wang, Q., Zhao, X., Liu, W., Zhang, Z.: Coercivity enhancement and microstructural optimization in diffusion-processed Ce-Nd-Fe-B-based films. Thin. Solid. Films. **645**, 1–4 (2018)

23. Govea-Alcaide, E., Machado, I.F., Bertolete-Carneiro, M., Muné, P., Jardim, R.F.: J. Appl. Phys. **112**, 113906–13913 (2012)